Highly Accurate Time-of-Flight Measurement Technique Based on Phase-Correlation for Ultrasonic Ranging

Md. Omar Khyam, Shuzhi Sam Ge, *Fellow, IEEE*, Xinde Li, *Senior Member, IEEE*, and Mark R. Pickering, *Member, IEEE*

***Abstract*— Ultrasonic-based distance measurements using time-of-flight (TOF) is a fundamental technique for different applications across a wide variety of fields. In general, cross correlation between a transmitted and received signal is considered to be the optimal TOF estimation technique, which produces a peak at the time delay between them. Cross correlation provides a superior performance in conjunction with a linear chirp. However, as its accuracy depends on the width of the peak, which is inversely proportional to the signal's bandwidth, it can only be said to be highly accurate if the reflected signal at the receiver is separated in time by more than the width of the correlation peak; otherwise, errors are introduced into the system. To improve its accuracy, the bandwidth of the transmitted signal must be increased, which increases the system cost. In this paper, to solve this problem, a threshold-based phase-correlation technique is proposed, which is able to provide a much narrower peak than cross correlation without increasing the signal's physical bandwidth. To evaluate the proposed method, in a controlled environment, two experiments were performed under low and high multipath conditions. For an operational range of 600 mm (indoor), the root-mean-square errors were [0.10, 0.56] mm and [0.19, 1.19] mm for low and high multipath environments, respectively, which indicate that the proposed technique is precise enough to support high accuracy applications.**

***Index Terms*— Correlation technique, time-of-flight (TOF) estimation, ultrasonic wave, distance measurement.**

I. Introduction

ULTRASONIC-BASED distance measurements using time-of-flight (TOF) techniques have been extensively used in research and production fields in many and varied applications, such as indoor positioning, [1]–[11], robot navigation [12]–[19], laparoscopic surgery [20], human pose estimation [21]–[28], and many industrial applications e.g., ultrasonic defects inspection [29], [30]. The general rationale for the system presented in this paper is the opportunity offered by ultrasound to conceive rather simple measurement methods or build comparatively cheap meters characterized by suitable accuracy, reduced measurement time and, above all, a high level of inherent safety [31].

The process of obtaining distance information is begun by sending an ultrasonic (US) burst from a transmitter to a receiver. Ideally, one would send a continuous wave signal, for instance, a sine wave, from the transmitter. Then, using the phase-shift information between the transmitted and received signals, the distance information could be obtained. This technique can measure distances up to a wavelength (λ) because a phase variation of a signal from 0° to 360° corresponds to a distance variation from 0 to λ. However, if the measured distance is longer than a wavelength, this technique is limited to short-range applications. Because the integer number of wavelengths within the distance is unknown.

Therefore, for distances longer than a wavelength, it is common to measure the TOF which employs the following concept. A transmitter sends an US pulse which travels through the air to a receiver and this traveling time (t_F) is used to obtain the distance (d) between the transmitter and receiver using the common, straightforward law [32]:

$$d = vt_F \tag{1}$$

where v is the speed of sound.

The simplest way of determining the TOF involves transmitting and detecting the arrival of an US signal by triggering the event when the received signal exceeds a predefined threshold level for the first time which, of course, must be above the noise level. Although it is computationally simple and can be implemented with low-cost single frequency US transducers, for low signal-to-noise ratio (SNR) signals, it is not the most suitable method because, on average, it estimates a false positive TOF compared with the actual one [31].

A more standard and proper TOF estimation technique is cross-correlation in which transmitted and received signals are cross-correlated to produce the maximum value at the time delay and performs better than the threshold technique for low SNR signals. It is considered as the optimal TOF estimation technique as it uses all the information contained in the signals [31] and gives the optimal weight to each frequency

Manuscript received July 29, 2016; revised October 28, 2016; accepted November 6, 2016. Date of publication November 21, 2016; date of current version December 20, 2016. This work was supported by the A*STAR Industrial Robotics Program, Singapore, under Grant R-261-506-007-305. The associate editor coordinating the review of this paper and approving it for publication was Prof. Z. Ignjatovic.

M. O. Khyam is with the Faculty of Engineering, Department of Electrical and Computer Engineering, National University of Singapore, Singapore 117580 (e-mail: fahad_ete@yahoo.com).

S. S. Ge is with the Social Robotics Laboratory, Department of Electrical and Computer Engineering, Interactive Digital Media Institute, National University of Singapore, Singapore 117576 (e-mail: samge@nus.edu.sg).

X. Li is with the Key Laboratory of Measurement and Control of CSE, Ministry of Education, School of Automation, Southeast University Nanjing 210096, China (e-mail: xindeli@seu.edu.cn).

M. R. Pickering is with the School of Engineering and Information Technology, University of New South Wales, Campbell, ACT 2612, Australia (e-mail: m.pickering@adfa.edu.au).

Digital Object Identifier 10.1109/JSEN.2016.2631244

component. The accuracy of cross-correlation depends mainly on the width of the correlation peak which is inversely proportional to the bandwidth, that is, the narrower the peak, the higher the TOF estimation accuracy. So a larger bandwidth translates to a higher accuracy although this results in an increased system cost. Above all, this technique can be said to be highly accurate if the reflected or multipath signal at the receiver is separated in time by more than the width of the correlation peak [33], [34] which might not always happen in an indoor environment due to the presence of numerous obstacles which can introduce errors into the system.

Therefore, to tackle this problem most of the ultrasonic systems [34]–[36] use broadband ultrasonic chirp signal which increases system cost. On the other hand, when ultrasonic systems use a narrowband chirp, they use interpolation techniques, as in [10] and [37], fitting the correlation sequence in the proximity of a peak to parabolic law and finding its maximum, which do not always provide the accurate estimation of the TOF. Super-resolution methods have also been proposed in [38] and [39] to determine TOF in a close multipath condition which computational complexity is extensive.

In this paper, a threshold-based phase-correlation technique is proposed which is able to provide a much narrower peak (a sharp peak) than cross-correlation without increasing the signal's physical bandwidth. Thus, it not only helps to accurately determine the TOF in an environment in which close multipath reflections occur but can also separate the individual multipath components.

The remainder of this paper is organized as follows: in Section II a linear chirp signal is introduced and a general system model required to illustrate the propagation of the chirp signal is described; the cross-correlation method in the frequency domain is discussed in Section III; our proposed threshold-based phase-correlation technique is explained in Section IV along with a comparison of the performances of the cross-correlation and proposed methods from simulations; Section V describes the experimental procedure for determining the accuracy of the proposed system along with the experimental results; and Section VI presents the conclusions drawn from this study and outlines future research.

II. Linear Chirp Signal

A linear chirp is represented by the bandpass signal:

$$s_T(t) = \begin{cases} \cos(2\pi(f_c t \pm \kappa \frac{t^2}{2})) & \text{for } -\frac{\tau}{2} < t < \frac{\tau}{2} \\ 0 & \text{otherwise} \end{cases} \quad (2)$$

where f_c is the centre frequency in Hz, $\kappa = \frac{B}{\tau}$ is the chirp rate (where B is the bandwidth in Hz and τ the signal duration in seconds) that sweeps the frequencies in the interval $[f_c - B/2, f_c + B/2]$, confirming B centered at frequency f_c.

A system model is required to illustrate the propagation of the chirp signal. The ideal propagation model takes only into account the direct-path signal. However, in indoor environments, a receiver receives multiple delayed and attenuated replicas of the transmitted signal due to reflections of the wavefront from multiple objects presented in the indoor environment. Therefore, for indoor environments, the received signals are often described mathematically as:

$$s_R(t) = s_T(t) * h(t) + w(t) \quad (3)$$

where $h(t)$ represents the impulse responses of the indoor environment (channel) and $w(t)$ the additive white Gaussian noise (AWGN) in the channel.

The impulse response $h(t)$ is modelled as the sum of $L+1$ impulses corresponding to the direct path with propagation delay t_{F_0} and L other possible paths between transmitter and receiver as:

$$h(t) = \sum_{j=0}^{L} A_j \delta(t - t_{F_j}) \quad (4)$$

where A_j represents the amplitude of the j-th ray, $\delta(t - t_{F_j})$ the propagation delay between the transmitter and receiver, ray $j = 0$ the direct path and $j > 0$ the multipath between a transmitter and receiver, $t_{F_j} = d_j/v$, where d_j is the distance travelled by ray j and v the speed of sound which depends on environmental factors such as temperature, pressure and humidity. Although the effect of pressure and humidity is negligible in indoor environments, the variability of the speed of sound with air temperature needs to be considered.

Unlike an electromagnetic signal, the speed of an ultrasonic signal is directly affected by the air temperature. As the distance between a transmitter and receiver is directly related to the speed of sound, in indoor environments, the variability of the speed of sound according to the air temperature needs to be considered, with the relationship between the speed of sound and air temperature given by:

$$v = (331.3 + 0.6\phi) \text{ m/s} \quad (5)$$

where ϕ is the ambient temperature in °C. This variability needs to be accounted for via calibration before any TOF measurements are taken. Generally, for TOF estimations, the cross-correlation method is used. The mathematical model of this method in the frequency domain is presented as follows.

III. Frequency Domain Cross-Correlation

Let the time domain transmitted and received signals are $s_T(t)$ and $s_R(t)$ respectively. Now using the Fourier transform, $s_T(t)$ and $s_R(t)$ can be described by a complex function of frequency as follows:

$$S_T(f) = \Im(s_T(t)) = A_T(f)e^{j\theta_T(f)} \quad (6)$$

$$S_R(f) = \Im(s_R(t)) = A_R(f)e^{j\theta_R(f)} \quad (7)$$

where $\Im$ denotes the Fourier transform operation and, A and θ represents the amplitude and phase of the complex frequency components of each signal respectively. Now, the cross-correlation of the transmitted and received signals in the frequency domain is:

$$\begin{aligned} C(f) &= S_T^*(f)S_R(f) \\ &= A_T(f)A_R(f)e^{-j\theta_T(f)}e^{j\theta_R(f)} \\ &= A_T(f)A_R(f)e^{j(\theta_R(f)-\theta_T(f))} \end{aligned} \quad (8)$$

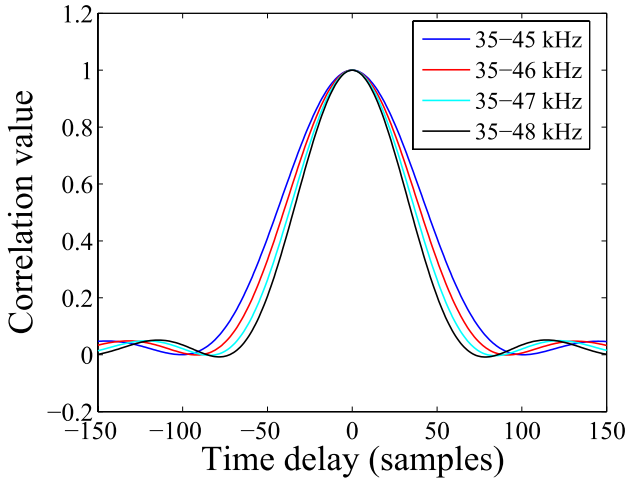

Fig. 1. Effect of bandwidth on cross-correlation width.

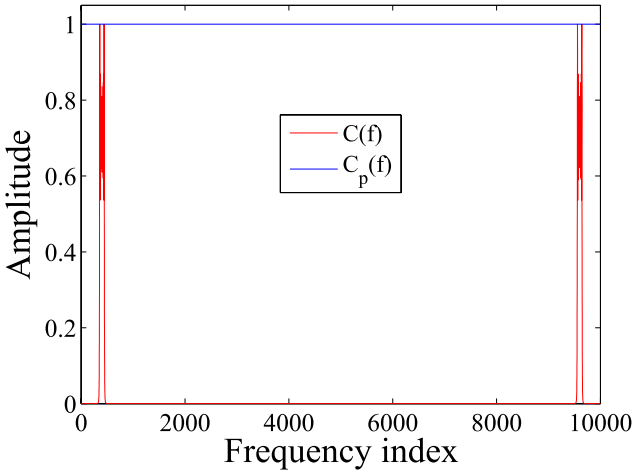

Fig. 2. Frequency spectrum of $C(f)$ and $C_p(f)$ for [35-45] kHz/10 ms Chirp sampled at 1 MHz.

where $*$ denotes the complex conjugate. The inverse Fourier transform of $C(f)$ represents the cross-correlation output as:

$$c(t) = \Im^{-1}(C(f)) = \Im^{-1}(A_T(f)A_R(f)e^{j(\theta_R(f)-\theta_T(f))}) \quad (9)$$

where $\Im^{-1}$ is the inverse Fourier transform. This cross-correlation provides a signal with a maximum value when the transmitted and received signals are perfectly aligned in time assuming no noise into the system.

The inverse Fourier transform of the exponential function (i.e., equation (9)) of a single frequency component is a sine function which gradually becomes a sinc function if the number of frequency components is increased and, finally, a delta function for an infinite number of frequency components. Therefore, it can be said that, by increasing the number of frequency components, i.e., the signal's bandwidth, the output from the cross-correlation ($c(t)$) can be narrowed, with the correlation width (ΔT) inversely proportional to the bandwidth (B) of the signal, i.e.,

$$\Delta T \propto \frac{1}{B} \quad (10)$$

as shown in Fig. 1.

Therefore, by increasing the bandwidth (B), one can reduce the width of the peak which means that system accuracy is improved because reflected paths will be more easily separable with wide band chirps. The problem here is that increasing the system bandwidth will increase the system cost. Therefore, in the following section, a phase-correlation technique which is able to provide a sharp peak without physically increasing the bandwidth is proposed.

IV. Proposed Method

A. Phase-correlation Method

According to equation (9), the cross-correlation output will be a delta function, i.e., approximately zero everywhere except at the position of time delay if each frequency index of $C(f)$ has a value, i.e., an infinite bandwidth. This could possibly be achieved virtually, without physically increasing the bandwidth, by modifying equation (8) as:

$$C_p(f) = e^{j(\theta_R(f)-\theta_T(f))} \quad (11)$$

This equation means that all the frequency spectrum of $C_p(f)$ has a unity magnitude whereas $C(f)$ has particular values at the transmitted frequency components as shown in Fig. 2. Therefore, in the ideal case (i.e., in a noiseless environment) the inverse Fourier transform of phase difference given in the following equation is a delta function which produces a peak at the minimum phase difference between the transmitted and received signals as it has a value at all frequency components.

$$c_p(t) = \Im^{-1}(C_p(f)) = \Im^{-1}(e^{j(\theta_R(f)-\theta_T(f))}) \quad (12)$$

However, in a real scenario, noise will be added with the received signal. Therefore, in that case, the inverse Fourier transform of the phase difference i.e., $c_p(t)$ will not be a shifted delta function because the phase will be: i) corrupted by the noise inside the pass band and ii) completely random (i.e., no useful information) outside the pass band as we have given the same weight to the phase of the frequency components inside and outside the pass band. However, in the presence of noise $c_p(t)$ will produce a sharp peak at the minimum phase difference between the transmitted and received signals and it would be detectable if it is above the noise level. Hence, we can say that performance of the phase-correlation estimator is highly dependant on the amount of noise contributing to the received signal, i.e., the SNR of the received signal. Fig. 3 shows the effect of the received signal's SNR on cross- and phase-correlations i.e., $c(t)$ and $c_p(t)$ (which was calculated using equation (13) that can be defined as the ratio of the square of the correlation main peak amplitude to the variance of the correlation noise).

$$\mathrm{SNR}_{\mathrm{Corr}} = 20\log\frac{\left|\mathrm{Corr}_{(\text{main peak})}\right|^2}{\mathrm{Var}(\mathrm{Corr}_{\mathrm{noise}})} \quad (13)$$

In this equation Var() represents the variance, $\mathrm{Corr}_{(\text{main peak})}$ the main peak of $c_p(t)$ and $c(t)$ in noiseless environment and, except the main peak of $c_p(t)$ and $c(t)$ in a noisy environment, all other components are $\mathrm{Var}(\mathrm{Corr}_{\mathrm{noise}})$. In Fig. 3, it has been noticed that the received signal's SNR has lower impact on cross-correlation than phase-correlation. This is because, phase-correlation gives the same weight to the phase of the

TABLE I
RMSE AT DIFFERENT SNRS WHEN DIRECT AND REFLECTED PATHS ARE WELL SEPARATED IN TIME (mm)

Methods	SNR in dB															
	5	6	7	8	9	10	11	12	13	14	15	16	17	18	19	20
Proposed	13.64	11.32	0.22	0.18	0.28	0.21	0.39	0.26	0.45	0.67	0.56	0.63	0.56	0.44	0.35	0.59
Cross-correlation	0.24	0.38	0.56	0.12	0.48	0.29	0.66	0.38	0.40	0.15	0.35	0.68	0.26	0.25	0.48	0.58

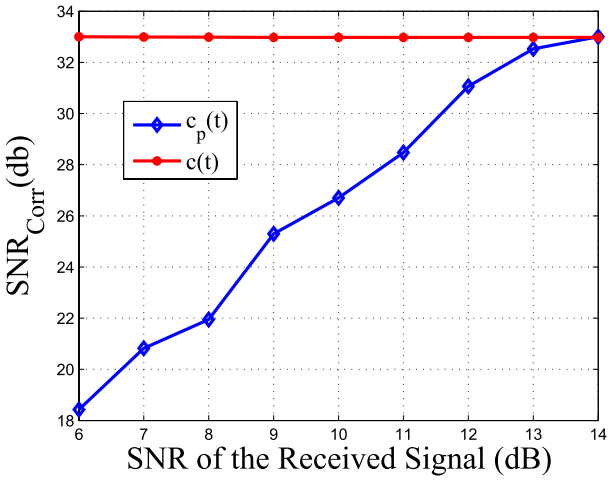

Fig. 3. Effect of received signal's SNR on cross- and phase-correlations.

frequency components of the signal inside and outside the pass band (in equation (11)) whereas the cross-correlation method gives the optimal weight to each frequency component (in equation (8)). However, at the same time in Fig. 4 (obtained using equations (9) and (12) when the received signal's SNR was 15 dB) shows that phase-correlation has a much narrower peak than cross-correlation hence, will allow the time delay between the transmitted and received chirps to be measured with greater precision than when using the cross correlation.

It is important to note that, in close multipath reception, the peak generated by the reflected path may exceed the main peak of $c_p(t)$ due to noise. In addition to this, the peak associated with the correct delay is not always the highest peak. In some cases, the direct path can experience attenuation, giving it a lower phase-correlation peak than indirect multipaths. In other cases, a number of indirect paths can combine to produce a peak that is greater than the one associated with the direct path. Herein, a threshold-based search mechanism is applied to find the earliest arriving phase-correlation peak above the noise floor. The earliest peak is assumed to belong to the direct path that gives the correct TOF. The threshold was set to 70% of the peak height of phase-correlation as that value was found to be high enough (in simulation and experiments) to detect the early peak above the noise floor at moderate SNRs and sufficiently low to guarantee detection of the direct path peak, even with strong reflections.

In summary, the proposed phase-correlation method is as follows.

1) Calculate the Fourier transform of the transmitted signal, i.e., $S_T(f) = A_T e^{j\theta_T}$.
2) Calculate the Fourier transform of the received signal, i.e., $S_R(f) = A_R e^{j\theta_R}$.
3) Calculate the angle difference between the received and transmitted signals, i.e., $\Delta\theta = (\theta_R - \theta_T)$.
4) Calculate the exponential of $\Delta\theta$, i.e., $C_p(f) = e^{j\Delta\theta}$.
5) Calculate the inverse Fourier transform of $C_p(f)$, i.e., $c_p(t) = \Im^{-1}(C_p(f))$.
6) Calculate the maximum value of $c_p(t)$.
7) Set a threshold to 70% of the maximum value of $c_p(t)$.
8) Find the position of $c_p(t)$ that exceed the predefine threshold which corresponds to the TOF (in sample).

To visualize how threshold-based phase-correlation works better than cross-correlation in a close multipath but in a moderate SNR (SNR>6) environment an example is demonstrated below.

B. Understanding Phase-Correlation Using an Example

The following examples provide a performance comparison in term of accuracy at different aspects (i.e., relative delay between direct and reflected paths and, the received signal's SNR). In this example, two cases are considered where at sampling frequency of 1 MHz, a linear chirp [35-45] kHz/10 ms (i.e., the length of the linear chirp is 10 ms and, its initial and final frequencies are 35 kHz and 45 kHz respectively) was created for transmission which was also used during the real experiment.

In the first case, the receiver receives the transmitted chirp with separation between the direct and reflected paths larger than the cross-correlation width ($\triangle T$) , which are, 1500 samples and 1950 samples which correspond to 51.6 cm and 67.08 cm respectively when the speed of sound is 344 m/s at 21 °C, with the corresponding path loss considered using reflection coefficients of 0.9. A reflection coefficient of 0.9 means that 10% of the signal's energy is lost upon reflection which indicates that the multipath effect is more intense at a higher reflection coefficient, and vice-versa. In this case, it is assumed that the channel was subjected to additive white Gaussian noise (AWGN) with SNR 5 dB to 20 dB with 1 dB gaps. The aim was to calculate the TOF. For each noise label, the simulation was run for a length of 1000 iterations. The RMSE from this simulation using the threshold-based phase-correlation and cross-correlation methods are compared in Fig. 5(a) and Table I. In these results, it has been noticed that, above 6 dB of SNR, the RMSE from the threshold-based phase-correlation method is almost constant within [0.18, 0.67] mm because, above this SNR, it (the phase-correlation method) produced a sharp peak at the minimum phase difference between the transmitted and received signals which was detectable with almost constant accuracy as it (the peak) was above the noise floor (an example shown in Fig. 6(d)). It has also been noticed that, below 6 dB of SNR, the accuracy from the threshold-based

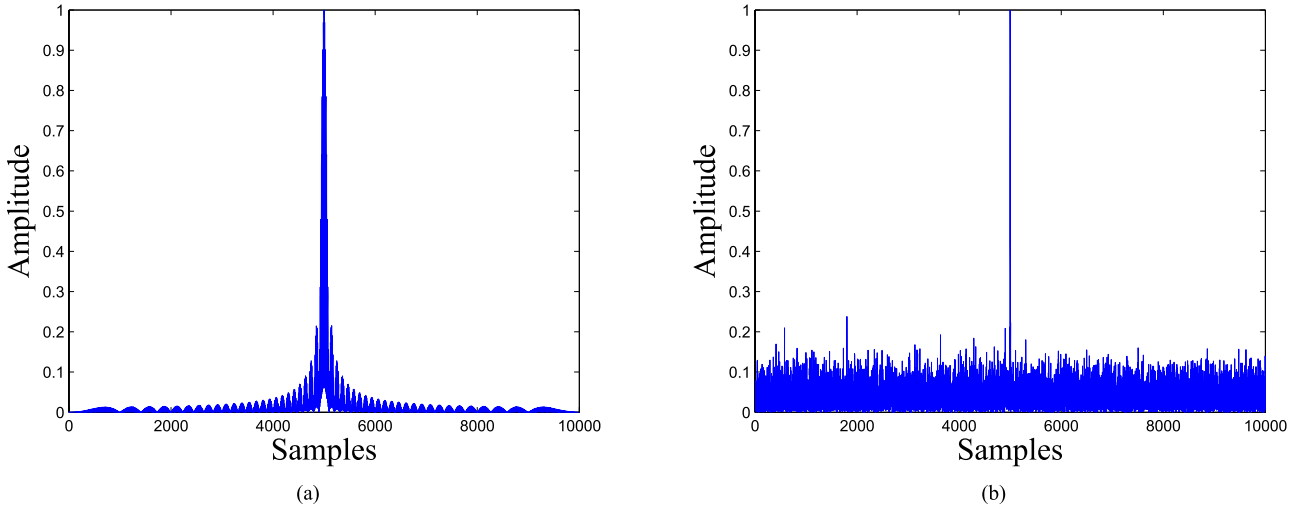

Fig. 4. Width of [35-45] kHz/10 ms chirp sampled at 1MHz for: (a) cross-correlation and (b) phase correlation.

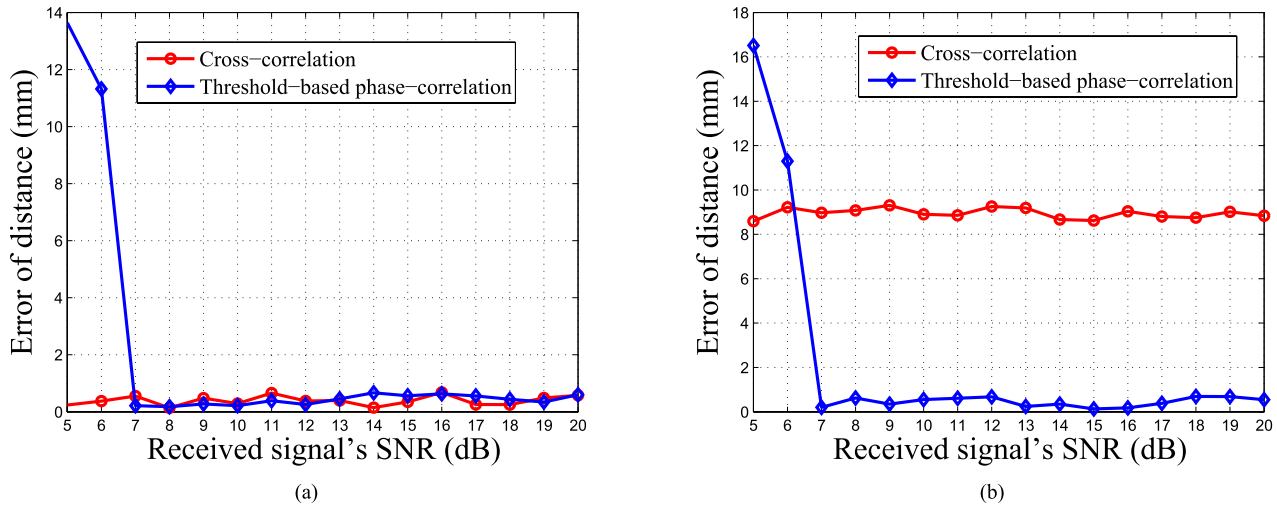

Fig. 5. Error for different SNR for cross-correlation and threshold-based phase correlation when direct and reflected paths are: (a) well separated in time and (b) close in time.

phase-correlation method degraded abruptly because below that SNR the peak generated at TOF was below the noise floor which was not detectable (an example shown in Fig. 6(b)). Therefore, it can be said that, the phase-correlation method highly depends on received signal's SNR as it gives the same weight to the phase of the frequency components of the signal inside and outside the pass band (in equation (11)). On the other hand, the RMSE from the cross-correlation technique is almost constant within [0.12, 0.68] mm even at low SNR as it gives the optimal weight to each frequency component (in equation (8)).

An example from this simulation is illustrated in Fig. 6 for the most noisy (SNR=5 dB) and best (SNR=20 dB) cases which indicates that both methods can estimate the direct path, i.e., the TOF and the reflected path accurately for the best case. However, for the most noisy case, the threshold-based phase-correlation method fails to detect the direct path, i.e., the TOF, and the reflected path whereas cross-correlation has the ability to detect both paths.

In the second case, the receiver receives the transmitted chirp with separation between the direct and reflected paths smaller than the cross-correlation width ($\triangle T$), which are, 1500 samples and 1555 samples which correspond to 51.6 cm and 53.49 cm respectively when the speed of sound and temperature are the same as in case-1. For the same environment as in case-1, the RMSE using the threshold-based phase-correlation and cross-correlation methods are compared in Fig. 5(b) and Table II. The results show that, the behaviour for the threshold-based phase-correlation method is almost the same as in case-1 for the same reason described in case-1 but, for the cross-correlation there is always an approximately constant error of [8.59, 9.31] mm as in this case the reflected path directly affected the correlation's main peak.

An example from this simulation is illustrated in Fig. 7 for the most noisy (SNR=5 dB) and best (SNR=20 dB) cases. This Figure indicates that for all SNRs, the peak for the reflected path is not visible in the cross-correlation output which means that the reflected path directly affected the correlation's width and its peak is generated at a false position with an error of 27 samples, which corresponds to 0.93 cm. On the other hand, although there is no defined peak in phase-correlation for the most noisy case, two distinct spikes are visible at exactly the

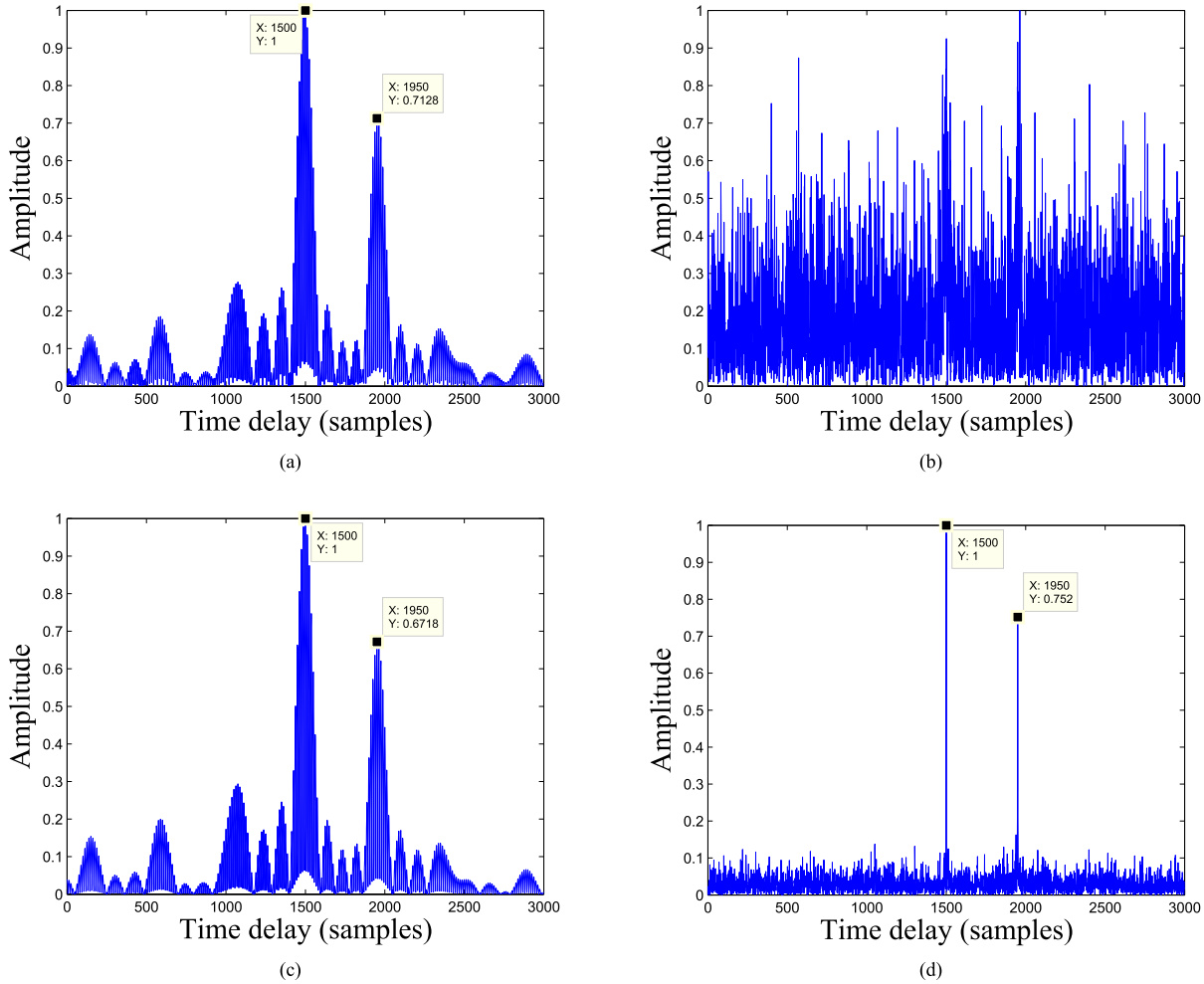

Fig. 6. Outputs when direct and reflected paths are well separated in time from cross-correlation and phase-correlation: (a), (b) at SNR 5 dB and (c), (d) at SNR 20 dB

TABLE II

RMSE AT DIFFERENT SNRS WHEN DIRECT AND REFLECTED PATHS ARE CLOSE IN TIME (mm)

Methods	SNR in dB															
	5	6	7	8	9	10	11	12	13	14	15	16	17	18	19	20
Proposed	16.51	11.30	0.20	0.62	0.35	0.55	0.61	0.68	0.25	0.35	0.13	0.18	0.38	0.69	0.69	0.54
Cross-correlation	8.59	9.22	8.97	9.08	9.31	8.90	8.86	9.25	9.19	8.67	8.62	9.04	8.81	8.75	9.0	8.8383

same positions of the direct and reflected paths for the best case.

Therefore, it can be said that phase-correlation has the ability to provide precise results in moderate SNR (>6 dB) and highly multipath environments, and can be applied in such applications which require high accuracy.

In this section, the behavior of threshold-based phase-correlation and cross-correlation techniques are described through simulation at different SNRs for a fixed situation. The next section describes the behavior of the threshold-based phase-correlation and cross-correlation methods at different SNRs for an arbitrary situation.

C. Simulation Results

A customized environment was simulated in Matlab to evaluate the performance of the threshold-based phase-correlation and cross-correlation methods for distance measurement. The simulator was designed to build a virtual two-dimensional (2D) rectangular room with (top, left) and (bottom, right) coordinates as: (-5, d/2) and (d+5, $-d$/2) respectively, where d is the distance between the transmitter and receiver and is varied from 40 to 60 cm, with the receiver and transmitter positioned at (0, 0) and (d, 0) respectively. In the simulator, a fixed number of reflection points at different positions of the transmitter in the enclosed geometry was generated, as per the described system model. Measurements were taken at different positions inside the room for distances between 40 cm and 60 cm and each simulation was run for 1000 iterations.

The simulation was performed for different noise levels in a multipath environment (5 paths at random positions) with reflection coefficients of 0.9, and the corresponding signal's attenuation calculated using the formula $A = A_0\ e^{-\gamma d}$, where A_0 is the unattenuated amplitude of the propagating

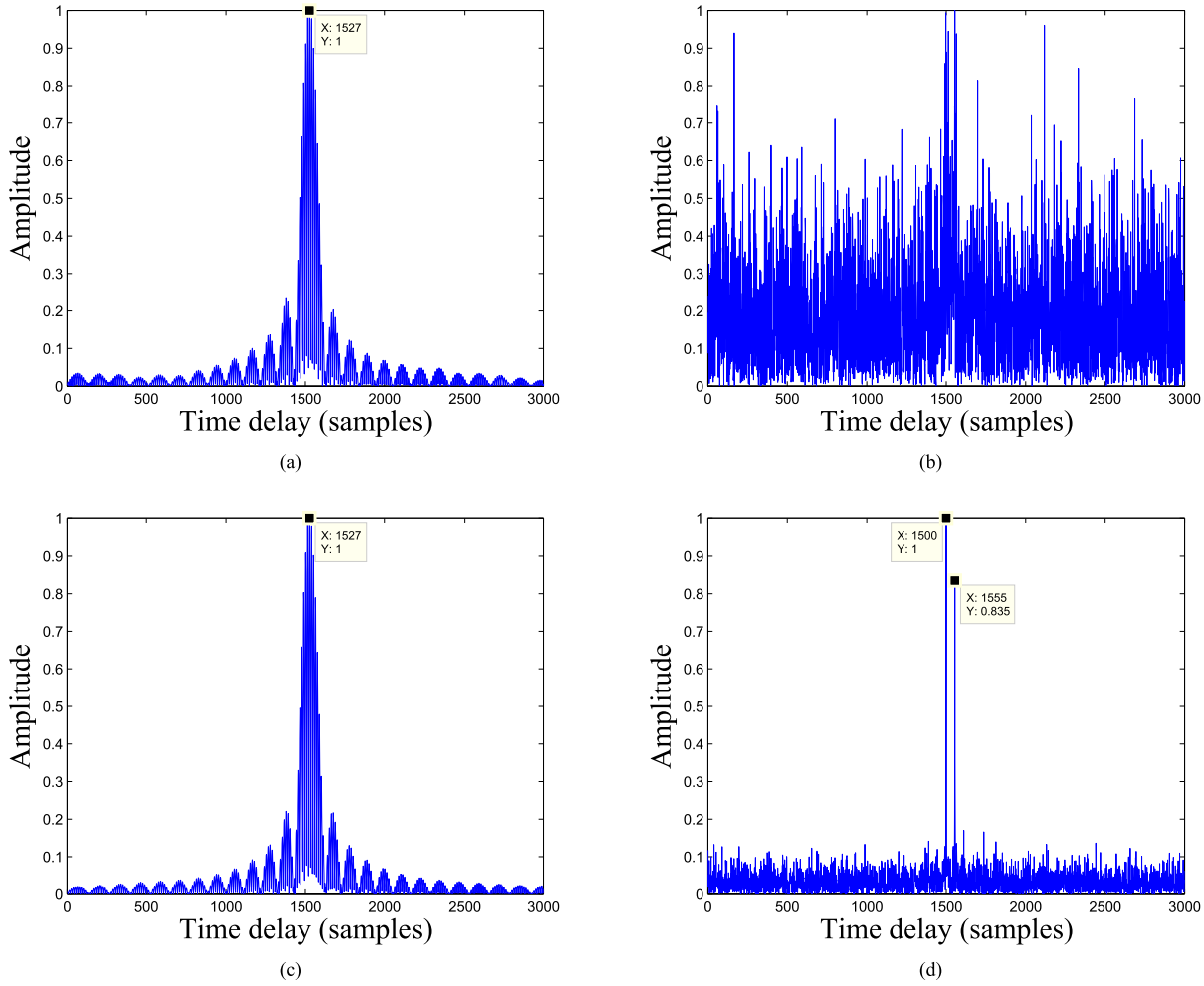

Fig. 7. Outputs when direct and reflected paths are close in time from cross-correlation and phase-correlation: (a), (b) at SNR 5dB and (c), (d) at SNR 20 dB

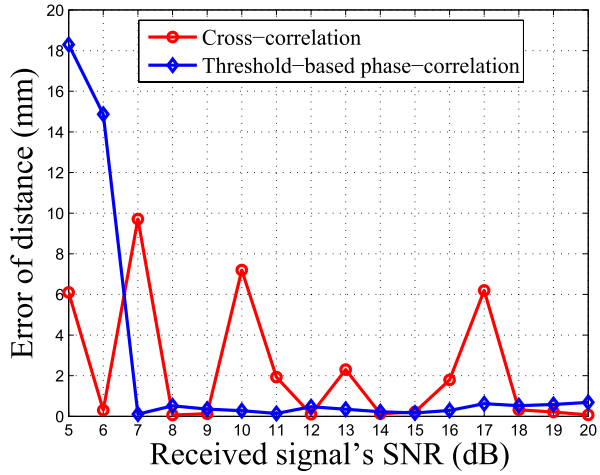

Fig. 8. Error for different SNRs for cross- and threshold-based phase-correlations in a random multipath environment.

wave at a location, A is the reduced amplitude after the wave has travelled a distance (d) from that initial location and γ is the attenuation coefficient of the traveling wave in the d direction. The parameters of the transmitted signal were chosen as [35-45] kHz/10 ms (sampled at 1 MHz)

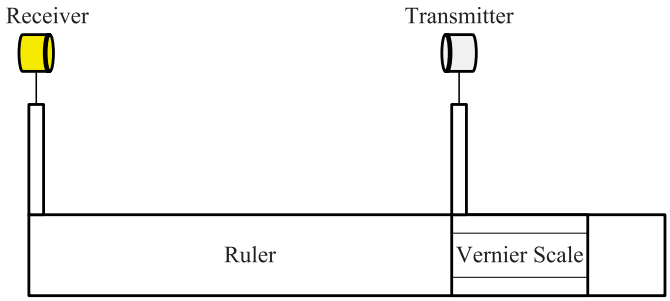

Fig. 9. Configuration of transmitter and receiver during distance measurement.

(which was also used during the real experiment), and the channel was subjected to AWGN with SNR 5 dB to 20 dB with 1 dB gaps.

Fig. 8 and its corresponding Table III represent the distance estimation accuracy obtained from the simulation measurements for the threshold-based phase-correlation and, cross-correlation methods. The results show that our system yields accurate and stable ranging results when the channel was subjected to SNR>6 dB whereas cross-correlation yields unstable results. This is because for SNR>6 dB, the proposed method provided a sharp peak at TOF even in a close multipath

TABLE III

RMSE AT DIFFERENT SNR IN A RANDOM MULTIPATH ENVIRONMENT (mm)

Methods	SNR in dB															
	5	6	7	8	9	10	11	12	13	14	15	16	17	18	19	20
Proposed	6.10	0.30	9.71	0.06	0.13	7.2	1.93	0.10	2.31	0.13	0.21	1.79	6.20	0.32	0.21	0.0700
Cross-correlation	18.30	14.87	0.11	0.52	0.35	0.27	0.14	0.47	0.34	0.23	0.16	0.30	0.62	0.52	0.58	0.69

TABLE IV

RMSE IN A LOW MULTIPATH ENVIRONMENT (mm)

Methods	Distance (mm)																				
	400	410	420	430	440	450	460	470	480	490	500	510	520	530	540	550	560	570	580	590	600
Proposed	0.17	0.10	0.56	0.30	0.48	0.54	0.45	0.10	0.37	0.13	0.41	0.19	0.18	0.19	0.32	0.34	0.11	0.41	0.49	0.14	0.33
Cross-correlation	0.47	0.51	0.47	0.26	0.50	0.49	0.30	0.19	0.42	0.42	0.22	0.29	0.48	0.22	0.26	0.39	0.17	0.33	0.15	0.23	0.51

TABLE V

RMSE IN A HIGH MULTIPATH ENVIRONMENT (mm)

Methods	Distance (mm)																				
	400	410	420	430	440	450	460	470	480	490	500	510	520	530	540	550	560	570	580	590	600
Proposed	1.14	0.48	0.96	1.09	0.64	0.40	0.97	0.96	0.30	0.69	0.97	0.19	0.75	0.56	1.18	0.56	0.68	0.56	1.08	0.99	1.19
Cross-correlation	0.31	0.93	6.21	0.02	3.33	0.89	5.32	0.17	1.24	0.59	1.056	1.19	0.74	0.50	8.13	0.24	0.04	0.51	9.17	0.71	0.92

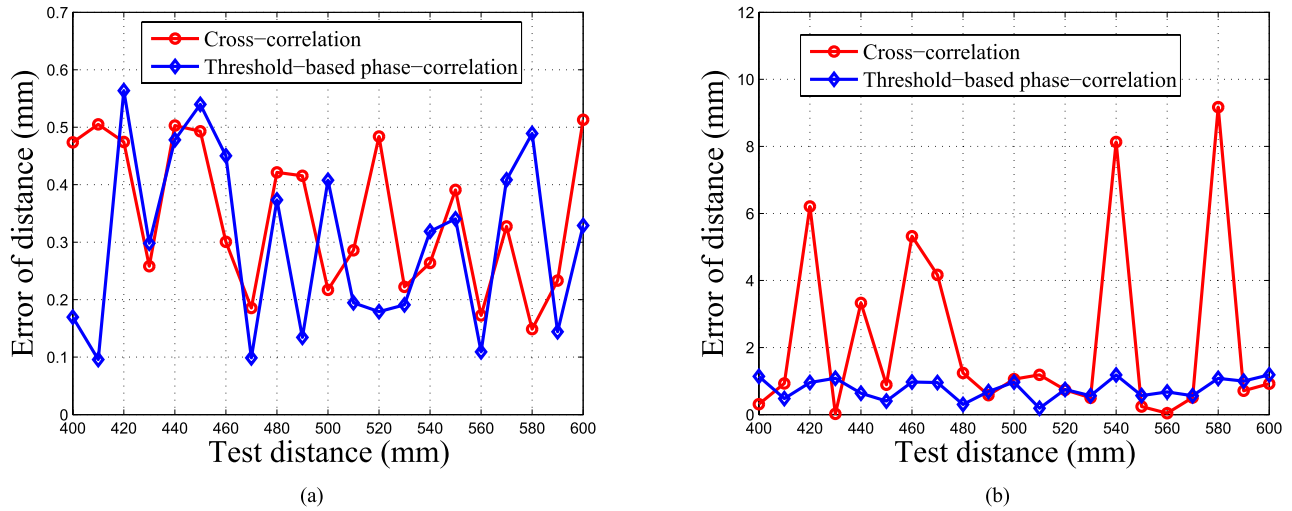

Fig. 10. Errors in distance measurement obtained from proposed and cross-correlation methods in: (a) low and (b) high multipath environments.

reception which was detectable with almost constant accuracy as it (the peak) was above the noise floor. In the cross-correlation method, the instability in accuracy occurred for those cases when separation between the direct and reflected paths was smaller than the cross-correlation's width which produced a peak at a false position. It is important to note that, when the channel was subjected to SNR$<$6 dB, the error from the proposed method exceeded that of the cross-correlation method. This is because the peak generated at the TOF by the proposed method was below the predefine threshold. Therefore, it can be said that phase-correlation has the ability to provide precise results in moderate SNR ($>$6 dB) and high multipath environment, and can be applied in such applications which require high accuracy.

V. EXPERIMENTS AND RESULTS

To evaluate the proposed method, a set of experiments were conducted according to the procedures described below. In these experiments, Piezotite MA40S4S and MA40S4R ultrasonic devices were used as transmitters and receivers which can effectively utilize 10 kHz of the frequencies centered around 40 kHz. To capture and digitize the transmitted and received signals and to measure the room temperature, a Measurement Computing USB-1604 DAQ module with a sampling rate of 1 Msample/s and a digital thermometer were used respectively. The transmitted signal was a linear chirp [35-45] kHz/10 ms.

In a controlled environment two experiments were performed under low and high multipath conditions to evaluate the proposed threshold-based phase-correlation technique for TOF estimation. A low multipath environment was created in a room by ensuring that there was no obstacles around the transmitter and receiver and both were placed at such a height that reflected waves from the ground and ceiling had a negligible effect on the received signal. On the other hand, a high multipath environment was created by placing different obstacles around the transmitter and receiver and both were placed at the center of a wooden table. In both experiments

the transmitter and receiver were attached to opposite ends of a ruler equipped with a Vernier scale with a precision of 0.05 mm (illustrated in Fig. 9). In both environments, the transmitter's positions were varied between 40 cm and 60 cm at intervals of 1 cm and the corresponding distances calculated by converting the TOFs obtained from the proposed method described in Section IV-A into distances. To demonstrate the improvement in accuracy obtained by the proposed approach, the distances were also calculated using the cross-correlation technique described in Section III for comparison. For every setting (i.e., different distances under different test cases), the experiments were repeated 50 times.

The RMSE from the experimental measurements for both low and high multipath environments using the proposed threshold-based phase-correlation and cross-correlation methods are compared in Fig. 10(a) and Fig. 10(b) with their corresponding data in Table IV and Table V respectively. In these results we can observe that in both environments our system produced accurate and stable ranging results whereas, although cross-correlation produced stable and accurate results for the low multipath environment, it produced unstable results for the high multipath environment (Fig. 10(b) and its corresponding Table V). This instability in cross-correlation occurred for those cases when the separation between the direct and reflected paths was smaller than the width of the cross-correlation peak.

VI. Conclusions and Future Work

In this paper, to determine the distance between a transmitter and receiver, a new threshold-based phase-correlation technique was proposed. The unique features of the proposed threshold-based phase-correlation approach compared with the cross-correlation technique are that: it has the capability to narrow the correlation peak by virtually rather than physically increasing the signal's bandwidth which not only helps to accurately determine the TOF in an environment in which close multipath reflections occur but can also separate the individual multipath components. It also reduces the system cost as it is not necessary to physically increase the signal's bandwidth. To evaluate the proposed method, in a controlled environment two experiments were performed under low and high multipath conditions. The experimental results showed that the proposed method was able to measure the distance between transmitter and receiver with significantly better accuracy than the alternative cross-correlation method. For an operational range of 600 mm (indoor), the RMSEs for the proposed and cross-correlation methods under low and high multipath conditions were [0.10, 0.56] mm, [0.19, 1.19] mm and [0.15, 0.51] mm, [0.17, 9.17] mm respectively which indicate that the proposed technique is precise enough to support high accuracy applications e.g., human movement analysis [40]–[42] and position measurement of laparoscopic tools during surgery [20].

It is worth noting that, although the threshold-based phase-correlation method achieves better accuracy than the cross-correlation method in a close multipath environment, which is a prerequisite for many high-accuracy applications, its accuracy highly dependents on the received signal's SNR. On the other hand, although cross-correlation provides lower accuracy in a close multipath environment, it outperforms the proposed method in low SNR environments. Therefore, our future work involves developing a joint estimation technique (i.e., combination of cross-correlation and threshold-based phase-correlation) to determine the TOF in a low SNR and close multipath environment.

Acknowledgment

The authors would like to thank the anonymous reviewers for their valuable comments.

References

[1] N. B. Priyantha, A. Chakraborty, and H. Balakrishnan, "The cricket location-support system," in *Proc. 6th Annu. Int. Conf. Mobile Comput. Netw.*, Aug. 2000, pp. 32–43.

[2] N. B. Priyantha, A. K. L. Miu, H. Balakrishnan, and S. Teller, "The cricket compass for context-aware mobile applications," in *Proc. 7th Annu. Int. Conf. Mobile Comput. Netw.*, 2001, pp. 1–14.

[3] A. Smith, H. Balakrishnan, M. Goraczko, and N. B. Priyantha, "Tracking moving devices with the cricket location system," in *Proc. 2nd Int. Conf. Mobile Syst., Appl. Services*, Jun. 2004, pp. 190–202.

[4] J. R. Gonzalez and C. J. Bleakley, "High-precision robust broadband ultrasonic location and orientation estimation," *IEEE J. Sel. Topics Signal Process.*, vol. 3, no. 5, pp. 832–844, Oct. 2009.

[5] A. Ward, A. Jones, and A. Hopper, "A new location technique for the active office," *IEEE Pers. Commun.*, vol. 4, no. 5, pp. 42–47, Oct. 1997.

[6] M. M. Saad, C. J. Bleakley, T. Ballal, and S. Dobson, "High-accuracy reference-free ultrasonic location estimation," *IEEE Trans. Instrum. Meas.*, vol. 61, no. 6, pp. 1561–1570, Jun. 2012.

[7] M. Alloulah and M. Hazas, "An efficient CDMA core for indoor acoustic position sensing," in *Proc. Int. Conf. Indoor Positioning Indoor Navigat.*, Sep. 2010, pp. 1–5.

[8] M. Hazas and A. Hopper, "Broadband ultrasonic location systems for improved indoor positioning," *IEEE Trans. Mobile Comput.*, vol. 5, no. 5, pp. 536–547, May 2006.

[9] C. Sertatıl, M. A. Altınkaya, and K. Raoof, "A novel acoustic indoor localization system employing CDMA," *Digit. Signal Process.*, vol. 22, no. 3, pp. 506–517, 2012.

[10] A. De Angelis *et al.*, "Design and characterization of a portable ultrasonic indoor 3-D positioning system," *IEEE Trans. Instrum. Meas.*, vol. 64, no. 10, pp. 2616–2625, Oct. 2015.

[11] A. Lindo, E. García, J. Ureña, M. del Carmen Pérez, and A. Hernández, "Multiband waveform design for an ultrasonic indoor positioning system," *IEEE Sensors J.*, vol. 15, no. 12, pp. 7190–7199, Dec. 2015.

[12] R. Zhang, F. Höflinger, and L. Reindl, "TDOA-based localization using interacting multiple model estimator and ultrasonic transmitter/receiver," *IEEE Trans. Instrum. Meas.*, vol. 62, no. 8, pp. 2205–2214, Aug. 2013.

[13] S. J. Kim and B. K. Kim, "Accurate hybrid global self-localization algorithm for indoor mobile robots with two-dimensional isotropic ultrasonic receivers," *IEEE Trans. Instrum. Meas.*, vol. 60, no. 10, pp. 3391–3404, Oct. 2011.

[14] S. J. Kim and B. K. Kim, "Dynamic ultrasonic hybrid localization system for indoor mobile robots," *IEEE Trans. Ind. Electron.*, vol. 60, no. 10, pp. 4562–4573, Oct. 2013.

[15] S.-I. Ko, J.-S. Choi, and B.-H. Kim, "Indoor mobile localization system and stabilization of localization performance using pre–filtering," *Int. J. Control, Autom. Syst.*, vol. 6, no. 2, p. 204, 2008.

[16] S. Widodo *et al.*, "Moving object localization using sound-based positioning system with doppler shift compensation," *Robotics*, vol. 2, no. 2, pp. 36–53, 2013.

[17] A. Yazici, U. Yayan, and H. Yücel, "An ultrasonic based indoor positioning system," in *Proc. Int. Symp. Innovations Intelli. Syst. Appl.*, Jun. 2011, pp. 585–589.

[18] T. Hori and Y. Nishida, "Improvement of position estimation of the ultrasonic 3D tag system," in *Proc. 17th IEEE Int. Symp. Robot Human Interactive Commun.*, Aug. 2008, pp. 436–441.

[19] A. Sanchez, A. de Castro, S. Elvira, G. Glez-de-Rivera, and J. Garrido, "Autonomous indoor ultrasonic positioning system based on a low-cost conditioning circuit," *Measurement*, vol. 45, no. 3, pp. 276–283, 2012.

[20] F. Tatar, J. R. Mollinger, J. Bastemeijer, and A. Bossche, "Time of flight technique used for measuring position and orientation of laparoscopic surgery tools," in *Proc. IEEE Sensors*, vol. 3, Oct. 2004, pp. 1480–1483.
[21] Y. Zejie, Y. Yanming, W. Qihang, and L. Wenlian, "A new system for three-dimensional kinematic trajectory acquisition and analysis—I. The application of an ultrasonic technique to human gait analysis," *Med. Eng. Phys.*, vol. 18, no. 5, pp. 420–426, 1996.
[22] Y. Zejie, Y. Yanming, L. Wenlian, and W. Qihang, "A new system for three-dimensional kinematic trajectory acquisition and analysis—II. Digital orthogonal integration phase-detection technique," *Med. Eng. Phys.*, vol. 18, no. 5, pp. 427–432, 1996.
[23] R. B. Huitema, A. L. Hof, and K. Postema, "Ultrasonic motion analysis system—measurement of temporal and spatial gait parameters," *J. Biomechan.*, vol. 35, no. 6, pp. 837–842, 2002.
[24] G. Ogris, T. Stiefmeier, H. Junker, P. Lukowicz, and G. Troster, "Using ultrasonic hand tracking to augment motion analysis based recognition of manipulative gestures," in *Proc. 9th IEEE Int. Symp. Wearable Comput.*, Oct. 2005, pp. 152–159.
[25] T. Stiefmeier, G. Ogris, H. Junker, P. Lukowicz, and G. Troster, "Combining motion sensors and ultrasonic hands tracking for continuous activity recognition in a maintenance scenario," in *Proc. 10th IEEE Int. Symp. Wearable Comput.*, Oct. 2006, pp. 97–104.
[26] T. Sato, S. Nakamura, K. Terabayashi, M. Sugimoto, and H. Hashizume, "Design and implementation of a robust and real-time ultrasonic motion-capture system," in *Proc. Int. Conf. Indoor Positioning Indoor Navigat.*, Sep. 2011, pp. 1–6.
[27] Y. Qi, C. B. Soh, E. Gunawan, K.-S. Low, and A. Maskooki, "A novel approach to joint flexion/extension angles measurement based on wearable UWB radios," *IEEE J. Biomed. Health Inform.*, vol. 18, no. 1, pp. 300–308, Jan. 2014.
[28] U. Yayan, H. Yucel, and A. Yazici, "A low cost ultrasonic based positioning system for the indoor navigation of mobile robots," *J. Int. Robot. Syst.*, vol. 78, no. 3, pp. 541–552, Jun. 2015.
[29] M. Siqueira, C. Gatts, R. D. Silva, and J. Rebello, "The use of ultrasonic guided waves and wavelets analysis in pipe inspection," *Ultrasonics*, vol. 41, no. 10, pp. 785–797, 2004.
[30] S. M. Tabatabaeipour and F. Honarvar, "A comparative evaluation of ultrasonic testing of AISI 316L welds made by shielded metal arc welding and gas tungsten arc welding processes," *J. Mater. Process. Technol.*, vol. 210, no. 8, pp. 1043–1050, 2010.
[31] R. Queiros, F. C. Alegria, P. S. Girao, and A. C. Serra, "Cross-correlation and sine-fitting techniques for high-resolution ultrasonic ranging," *IEEE Trans. Instrum. Meas.*, vol. 59, no. 12, pp. 3227–3236, Dec. 2010.
[32] R. Halmshaw, *Non-Destructive Testing*. London, U.K.: E. Arnold, 1997.
[33] K. Pahlavan, X. Li, and J.-P. Mäkelä, "Indoor geolocation science and technology," *IEEE Commun. Mag.*, vol. 40, no. 2, pp. 112–118, Feb. 2002.
[34] P. Misra, N. Kottege, B. Kusy, D. Ostry, and S. Jha, "Acoustical ranging techniques in embedded wireless sensor networked devices," *ACM Trans. Sensor Netw.*, vol. 10, no. 1, Dec. 2013, Art. no. 15.
[35] S. I. Lopes, J. M. N. Vieira, and D. Albuquerque, "High accuracy 3D indoor positioning using broadband ultrasonic signals," in *Proc. 11th IEEE Int. Conf. Trust, Security Privacy Comput. Commun.*, Jun. 2012, pp. 2008–2014.
[36] P. Lazik and A. Rowe, "Indoor pseudo-ranging of mobile devices using ultrasonic chirps," in *Proc. 10th ACM Conf. Embedded Netw. Sensor Syst.*, 2012, pp. 99–112.
[37] D. Marioli, C. Narduzzi, C. Offelli, D. Petri, E. Sardini, and A. Taroni, "Digital time-of-flight measurement for ultrasonic sensors," *IEEE Trans. Instrum. Meas.*, vol. 41, no. 1, pp. 93–97, Feb. 1992.
[38] H. Farrokhi, "Toa estimation using music super-resolution techniques for an indoor audible chirp ranging system," in *Proc. IEEE Int. Conf. Signal Process. Commun. (ICSPC)*, Nov. 2007, pp. 987–990.
[39] S. Yifeng, Z. Yongning, and W. Lei, "A fast estimation of multipath delay using chirp signal," in *Proc. Int. Conf. Commun. Mobile Comput. (CMC)*, vol. 2, Apr. 2010, pp. 510–514.
[40] R. M. Kiss, "Verification of determining the spatial position of the lower extremity by ultrasound-based motion analyser," *Periodica Polytechnica Civil Eng.*, vol. 51, no. 1, pp. 39–43, 2007.
[41] Y. Qi, C. B. Soh, E. Gunawan, and K. S. Low, "Ambulatory measurement of three-dimensional foot displacement during treadmill walking using wearable wireless ultrasonic sensor network," *IEEE J. Biomed. Health Inform.*, vol. 19, no. 2, pp. 446–452, Mar. 2014.
[42] M. W. Whittle, *Gait Analysis: An Introduction*. London, U.K.: Butterworth, 2014.

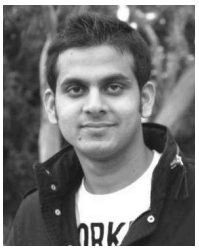

Md. Omar Khyam received the B.Sc. degree in electronics and telecommunication engineering from the Rajshahi University of Engineering and Technology, Rajshahi, Bangladesh, in 2010, and the Ph.D. degree from the University of New South Wales, Australia, in 2015. He is currently a Post-Doctoral Research Fellow with the National University of Singapore. His research interests include signal processing and wireless communication.

Shuzhi Sam Ge (S'90–M'92–SM'99–F'06) received the B.Sc. degree from the Beijing University of Aeronautics and Astronautics, Beijing, China, in 1986, and the Ph.D. degree from the Imperial College of Science, Technology and Medicine, University of London, London, U.K., in 1993. He is currently the Founding Director of the Robotics Institute and the Institute of Intelligent Systems and Information Technology, University of Electronic Science and Technology of China, Chengdu, China. He is also the Founding Director of the Social Robotics Laboratory, Interactive Digital Media Institute, National University of Singapore, Singapore, where he is a Professor with the Department of Electrical and Computer Engineering.

Dr. Ge is also the Editor-in-Chief of the *International Journal of Social Robotics*. He has served as an associate editor for a number of flagship journals. He has also served as the Vice-President of Technical Activities from 2009 to 2010, Membership Activities from 2011 to 2012, and the IEEE Control Systems Society.

Xinde Li (M'09–SM'16) received the Ph.D. degree in control theory and control engineering from the Department of Control Science and Engineering, Huazhong University of Science and Technology, Wuhan, China, in 2007. From 2012 to 2013, he was a Visiting Scholar with the School of Interactive Computing, Georgia Institute of Technology. In 2016, he was a Post-Doctoral Research Fellow with the Department of Electrical and Computer Engineering, National University of Singapore. He joined the School of Automation, Southeast University, Nanjing, China, where he is currently a Professor and a Ph.D. Supervisor. His research interests include information fusion, object recognition, computer vision, intelligent robot, and human–robot interaction. He received a Talent of Qing Lan Project Award of Jiangsu Province and a Six Major Top-talent Plan Award of Jiangsu Province, China.

Mark R. Pickering (S'92–M'95) was born in Biloela, Australia, in 1966. He received the B.Eng. degree in electrical engineering from the Capricornia Institute of Advanced Education, Rockhampton, QLD, Australia, in 1988, and the M.Eng. and Ph.D. degrees in electrical engineering from the University of New South Wales, Canberra, NSW, Australia, in 1991 and 1995, respectively.

He was a Lecturer from 1996 to 1999 and a Senior Lecturer from 2000 to 2009 at the School of Electrical Engineering and Information Technology, University of New South Wales, where he is currently an Associate Professor. His research interests include video and audio coding, medical imaging, data compression, information security, data networks, and error-resilient data transmission.